Ecosystem leaf area, gross primary production, and evapotranspiration responses to wildfire in the Columbia River Basin

Mingjie Shi[1], Nate Mcdowell[1], Huilin Huang[1], Faria Zahura[1], Lingcheng Li[1], and Xingyuan Chen[1]

[1]Pacific Northwest National Laboratory

March 15, 2024

Ecosystem leaf area, gross primary production, and evapotranspiration responses to wildfire in the Columbia River Basin

Mingjie Shi[1], mingjie.shi@pnnl.gov

Nate McDowell[1], nate.mcdowell@pnnl.gov

Huilin Huang[1], huilin.huang@pnnl.gov

Faria Zahura[1], fariatuz.zahura@pnnl.gov

Lingcheng Li[1], lingcheng.li@pnnl.gov

Xingyuan Chen[1]; xingyuan.chen@pnnl.gov

1. Pacific Northwest National Laboratory

Key words: Burn severity, Resistance, Resilience, Columbia River Basin, MODIS

Abstract

Wildfires impact the provision of ecosystem services and are increasing in intensity, frequency, and spatial area globally. The rate of vegetation recovery after fire plays a major role in the recovery of ecosystem services, but such recovery rates are poorly understood. Here we used remotely sensed data products from the Moderate Resolution Imaging Spectroradiometer (MODIS) to quantify the resistance and resilience of leaf area index (LAI), gross primary production (GPP), and evapotranspiration (ET) to 138 wildfires across the Columbia River Basin of the Pacific Northwest in 2015. Increasing burn severity caused lower resistance and resilience for all three variables. Resistance and resilience were highest in grasslands, intermediate in woodlands, and lowest in needleleaf evergreen forests, consistent with adaptation of these vegetation types to fire. LAI had consistently lower resistance and resilience than GPP and ET, which is consistent with physical and physiological mechanisms that compensate for reduced LAI. Resilience was influenced by precipitation, vapor pressure deficit (VPD), and burn severity across all three vegetation types, however, burn severity played a more minor role in grasslands. Increasing wildfire severity will reduce the resistance and resilience and lengthen the recovery time of vegetation structure and fluxes with climate change, with significant consequences on the provision of ecosystem services and complications for model predictions.

1. Introduction

Climate change has driven a global increase in the frequency and severity of wildfires (Jones et al. 2020; Pechony et al. 2010; Schoennagel et al., 2017; Westerling et al. 2016). Wildfires cause dramatic impacts on ecosystem carbon and water cycles that can last for decades (Adams et al., 2012; Bart et al. 2020). A primary mechanism underlying these responses is the loss of ecosystem-scale leaf area i.e., leaf area index (LAI), that reduces gross primary production (GPP) and evapotranspiration (ET) through lost photosynthetic and transpiring surface area and microclimate shifts. These large-scale changes in LAI, GPP, and ET cascade down to numerous consequences including reduced carbon storage and altered streamflow (McDowell et al. 2023; Seidl et al. 2014). The consistent predictions of increasing future wildfire frequency and severity due to climate change (Rammer et al. 2021; Wimberly et al. 2014; Williams et al. 2019) make improving our predictive understanding a particularly urgent science objective.

Model predictions of wildfire impacts on the carbon and water cycles are tenuous due to a lack of empirical quantification of the relationships between burn severity of wildfire and vegetation type (VT) with LAI, GPP, ET, and their rate of post-fire recovery (Poulos et al. 2021). Greater burn severity drives larger impacts and longer recovery times (e.g., Jin et al. 2012), which vary with the vegetation types (Hislop et al. 2019). VTs adapted to high fire frequencies, such as grasslands, should have more rapid recovery than those without such adaptations, such as needleleaf evergreen forests (Sun et al. 2020; Seidl and Turner 2022). LAI, GPP, and ET could also differ in their responses to fire via decoupling of LAI control over GPP and ET. Reductions in GPP and ET could be proportionately less than for LAI due to increases in photosynthesis and transpiration per unit leaf area in surviving plants driven by increased soil moisture and light (Whitehead 1998; Gough et al. 2013). Reduced ET due to suppressed canopy transpiration can be additionally compensated by increased soil evaporation (McDowell et al. 2023). However, decoupling of GPP and ET from LAI has not been studied in relation to wildfires nor at regional scales.

Resistance and resilience are two ecological concepts used to evaluate the impacts and responses of ecosystems to disturbances. Resistance is the degree of immediate impact on an ecosystem from a disturbance, and resilience is the capacity of a system to recover after the disturbance (Holling 1973; Zheng et al. 2021). Mathematically, resistance is calculated as (De Soto et al. 2020):

$$\text{Resistance} = \frac{A_{2016}}{\bar{A}_{2011-2014}} \qquad (1)$$

$$\text{Resilience} = \frac{\bar{A}_{2017-2020}}{\bar{A}_{2011-2014}} \qquad (2)$$

Where A represents the ecohydrological variables, LAI, GPP, and ET, used in this study, and the specific years are indicated in Equations (1) and (2). The use of these two conceptual models has yielded significant insights into disturbance impacts on forest composition, structure, survival, and growth (Albrich et al. 2020; De Soto et al. 2020).

There have been numerous studies on the ecosystem-scale impacts and recovery of wildfires (Balshi et al. 2009; Mills et al. 2015), but those have not used the framework in De Soto et al. (2020) by simultaneously examining the responses of LAI, GPP, and ET to fire disturbances, particularly in relation to burn severity and VTs. To investigate the coupled resistance and resilience of LAI, GPP, and ET, we examined the resistance and resilience of LAI, GPP, and ET in relation to wildfire severity and VTs (grasslands, woodlands, and forests) across the Columbia

River Basin (CRB) in the Pacific Northwest, USA. We used 2015 for our disturbance year because the CRB experienced particularly widespread fire occurrences in 2015 (Halofsky et al. 2020). Our research hypotheses were: (1) higher burn severity results in lower resistance and resilience across all VTs, (2) resistance and resilience are highest in grasslands, intermediate in woodlands, and lowest in forests, and (3) across all VTs resistance and resilience post-disturbance was highest for GPP and ET, and lowest for LAI. Because precipitation and vapor pressure deficit (VPD) influence vegetation growth in this semi-arid region, we also tested the hypothesis (4) that precipitation and VPD are more important to resilience in grassland than in other VTs. To test these hypotheses, we applied resistance and resilience algorithms (equations 1 and 2) to remotely-sensed LAI, GPP, and ET, and used the random forest feature importance method (Breiman, 2021) to investigate climate dependency.

2. Methods

In this section, we describe the data products and processing methods. The analyses were performed at spatial resolutions 500–1000 meters, and our research time frame is 2011–2020, which is centered around the time of maximum fire occurrence in the region (2015). We use the (1) Moderate Resolution Imaging Spectroradiometer (MODIS) land cover type (LCT; Sulla-Menashe et al. 2018) to identify surface VTs; (2) burn severity product from the Monitoring Trends in Burn Severity (MTBS) program to classify the location and severity of fires (Eidenshink et al. 2007); (3) the meteorological data from ECMWF Reanalysis Version 5 (ERA5) to quantify annual variation in climate (Hersbach et al. 2020); (4) the MODIS LAI (Myneni et al. 2002), GPP, and ET products (Running et al. 2004) to assess the ecosystem resistance and resilience due to fire disturbance. To interpret the essential factors controlling resilience of different VTs, the random forest feature importance method was used to assess the importance of precipitation, VPD, and burn severity to the resilience values in 2020 represented by LAI, GPP, and ET.

2.1 Characterizing surface vegetation types

In this research, we used the MODIS land cover type data set, MODIS MCD12Q1 version 6.1 (Sulla-Menashe et al. 2018; Friedl et al. 2022), to identify the surface VT. The spatiotemporal resolution of this data set is 500 meters and annual (Table 1). The VT map in 2015 showed that needleleaf evergreen forest (NEF), woody savannas (WDS), and grassland (GL), and croplands are the four dominant vegetation cover types over the CRB (Figure S1). In this study, we studied the impacts of wildfire over NEF, WDS, and GL.

2.2 Identifying the 2015 fire events

We identified all the 2015 fire events in the CRB so that we would have sufficient data both pre- and post-fire for calculating resistance and resilience, and because 2015 had the highest occurrence of fire events in this region during the time period of available remote sensing products. The MTBS (1984–present) maps burn extent and severity across the United States (Eidenshink et al. 2007; Picotte et al. 2020). MTBS includes all fires >= 4.05 km^2 in the western United States, where burn severity is quantified as visible alteration of vegetation, dead biomass, and soil that occurs within a fire perimeter (Eidenshink et al. 2007). Changes in vegetation and biomass damage resulting from fires were assessed using the Composite Burn Index (CBI). These changes are also correlated with remotely sensed estimates such as the differenced Normalized Burn Ratio (dNBR), a metric measuring the difference between pre- and post-fire NBR images (Eidenshink et al. 2007).

The burn severity product from MTBS is widely used as a viable estimate of burnt severity within certain ecosystems in the United States (Cansler and McKenzie 2012; Picotte et al. 2020).

The MTBS products include burn perimeters and burn severity, and we used the burn severity categories to identify fires and their features (e.g., burned area, burn severity) over the CRB. The MTBS data are at a 30-meter spatial resolution and upscaled to the 500-meter spatial resolution for the comparison with the MODIS data products (Table 1). Since MTBS uses different integers to represent burn severity categories, which use 1–4 to represent unburned to low, low, moderate, and high, respectively, the upscaling processes with the area-average re-mapping method generate floating numbers. Here, the numbers and meanings of burn severity values before and after the re-group are in Table S1. Based on this re-group method, the fire events and their burn severity in 2015 is shown in Figures S2a and S2c. To identify the vegetation type where each fire event occurred, we applied the MTBS fire boundary (i.e., shape) files describing the boundary of each fire event to the VT map (Figure S1). We then obtained the dominant VT of each fire event defined as the VT whose area accounts for more than 50% of burned area for that event. This analysis aimed to comprehend which VT(s) are predominantly affected by fire across the CRB (Figure S2b).

2.3 Interannual climate

We quantified interannual climate throughout the study region to determine if our resistance and resilience estimates were influenced by climatic variation. Here, we used precipitation, surface air temperature, and water vapor deficit (VPD) from ERA-5 (2011–2020; Hersbach et al. 2020). The data set is originally at the 30-kilometer spatial resolution, and we used the nearest-neighbor method to downscale the data to the 500-meter spatial resolution to match the spatial resolutions of other data sets (e.g., MODIS) of this study. The ten-year mean precipitation and surface air temperature are shown in Figure S3. We then used the MODIS LCT suggested VT and MTBS burn severity information in each 500-meter data pixel to group precipitation, surface air temperature and VPD within each fire disturbed region to their respective VT and then averaged the grouped climate variables for each VT. The specific process is the same to the MODIS LAI, GPP, and ET grouping, and more details of this method are introduced in the data description of MODIS data products of LAI, GPP, and ET.

2.4 Quantifying LAI, GPP, and ET

We used the MODIS LAI product at the 4-day interval and 500-meter spatial resolution (Myneni et al. 2002), and the MODIS GPP and ET products at the 8-day interval and 1000-meter spatial resolution (Running et al. 2004), which was downscaled to the 500-meter spatial resolution by using the nearest-neighbor method. To identify LAI, GPP, and ET changes among different VTs and burn severity categories, we applied the MTBS boundaries and MODIS LCT suggested VTs to the MODIS LAI, GPP, and ET products. To ensure the calculation accuracy, we evaluated the variations of these metrics by using MODIS VT pixels within the fire boundaries to group these variables based on VTs and calculated the means for the same VTs across all the fire boundaries. Specifically, the VT information in each MODIS pixel within different fire boundaries are applied to the corresponding data pixels of LAI, GPP, and ET, respectively. We then averaged LAI, GPP, ET of the same VT and with the same burn severity across all the 500-meter MODIS data pixels. As discussed above, ERA5 precipitation and temperature data are also grouped between different VTs by using this method. Thus, instead of considering the dominant VT in each fire boundary, we accurately performed the calculation, which could avoid the errors associated with the weights of each VT in different fire boundaries. All the above-mentioned calculation were performed during 2011–2020.

Table 1. The data products used in this research.

Data variables	Spatial resolution	Temporal resolution	Data time spans	Data sources	Reference
Precipitation	30 km	Monthly	1940–ps.	ERA5	Hersbach et al. (2020)
Surface air temperature	30 km	Monthly	1940–ps.	ERA5	Hersbach et al. (2020)
Water vapor deficit	30 km	Monthly	1940–ps.	ERA5	Hersbach et al. (2020)
Burn severity	30 m	Annual & event	1984–ps.	MTBS	Eidenshink et al. (2007)
Vegetation type	500 m	Annual	2002–ps.	MODIS	Sulla-Menashe et al. (2018)
LAI	500 m	4-day	2002–ps.	MODIS	Myneni et al. (2002)
GPP	1000 m	8-day	2002–ps.	MODIS	Running et al. (2004)
ET	1000 m	8-day	2002–ps.	MODIS	Running et al. (2004)

2.5 LAI, GPP, and ET based resistance and resilience calculations

We calculated post-fire resistance and resilience for LAI, GPP, and ET (Eqs (1) and (2); De Soto et al. 2020). We did not include 2015 values of LAI, GPP, or ET in the calculations because the fires happened mid-way through the growing season (Figure S4), thus the 2015 values include both pre- and post-fire, making them inappropriate for resistance and resilience calculations. Resilience can be calculated for each year post disturbance (e.g., De Soto et al. 2020). Given that resilience could exhibit interannual variations due to climate variations, we also calculated resilience for each individual year for all the VTs with various burn severity levels.

We used LAI, GPP, and ET observations from the growing season, which we defined as days with values larger than 30% of the annual maximum. This threshold number can be tweaked

(Shi et al. 2020), and we chose to use this value to avoid the MODIS data uncertainty during snow seasons. To avoid any error associated with using only a single observation, we identified the annual peak value and then averaged that value with records from the previous and subsequent eight days to generate the annual maximum value. This means that for MODIS LAI, with 4-day temporal resolution, we averaged five contiguous records centered around the peak value. For MODIS GPP and ET, with 8-day temporal resolution, we averaged three records, one before the peak, the peak itself, and one after the peak. To calculate the start and end of the growing seasons, we calculated the 4-record running mean (i.e., 16 days) of LAI and 2-record running mean (i.e., 16 days) of GPP and ET over the entire year. The start of each year's growing season was determined when the running mean exceeds 30% of the annual maximum value, and the end of growing season was calculated with the running mean dropped below 30% of the annual maximum. The growing season length based on different vegetation types with varied burn severity is shown in Figure S5.

2.6 Random forest feature importance

To interpret the factors controlling resilience of different VTs, the random forest feature importance method (Breiman, 2021) was implemented using the scikit learn package in python. Random forest uses a large collection of decision trees to predict the target variable based on its relationship with a specified set of input features. Each tree learns from a randomly chosen subset of samples and features, while the final prediction is made by averaging predictions from all trees. Furthermore, the algorithm reports the relative importance of input features by considering the reduction in impurity achieved by each feature during tree construction.

For this analysis, the random forest was trained with a set of input features that include burn severity in 2015, and total precipitation and mean VPD between 2017 and 2020, for each grid in the burn areas. Nine separate models were trained to predict three target variables: resilience for LAI, GPP and ET in year 2020 for NEF, WDS and GL. The number of samples in NEF, WDS and GL were 11,881, 15,684 and 26,840, respectively.

Random forest hyperparameters such as number of trees and number of features considered at splitting were predefined before model training. Here, number of trees was set to 100. The GridSearchCV algorithm from the scikit learn package was applied on 85% of randomly chosen samples to find the optimal number of features considered at splitting, and it was determined to be 1. Model training and testing were performed by splitting the samples randomly with 85% in training and 15% in testing. The random forest model was trained 100 times by performing 100 randomized splits to reduce any bias from splitting. From the 100 trained models, the distribution on train and test R^2 scores were obtained and the relative importance for each feature were averaged.

3. Results

3.1 The meteorological conditions and burn severity in CRB

For the 138 fire events in the CRB in 2015, we remove the areas that experienced fire in 2011–2014 or in 2016–2020, thus our resistance and resilience calculations are not confounded by repeat fires. August was the month with the highest fire frequency in 2015 with 91 fire events (Figure S2a). NEF experienced 42, WDS experienced 27, and grasslands experienced 67 fire events (Figures S1 and S2b). There were two fire events in croplands, which were excluded from further analyses.

Mean precipitation and surface air temperature over the Columbia River Basin were 789 ± 63 (mm year^{-1}) and 5.7 ± 0.7 (°C) during 2011–2020 (Figure S3). The spatial pattern of precipitation and surface air temperature suggest a relatively warmer and drier condition in the southern part of the basin, where the areas are mostly covered by grassland (Figure S1). The western and northeastern areas of the basin had higher precipitation, ranging from 700 to 1300 mm year^{-1}, and lower air temperatures, ranging from -3.0 to 11.0 (°C) (i.e., from the northernmost part to the central–southern part of CRB; Figure S3b). These areas have a greater proportion of NEF and WDS (Figures S1 and S3). We further examined the climate for each of the 138 fire locations broken into the three vegetation types. Climate conditions in 2015, the year of high fire activity, was particularly dry and warm across all vegetation types. There was no significant difference in mean annual precipitation and surface air temperature between 2011–2014 and 2016–2020 (Figure 1 and Table S2). Therefore, climate variations did not confound resistance and resilience calculations.

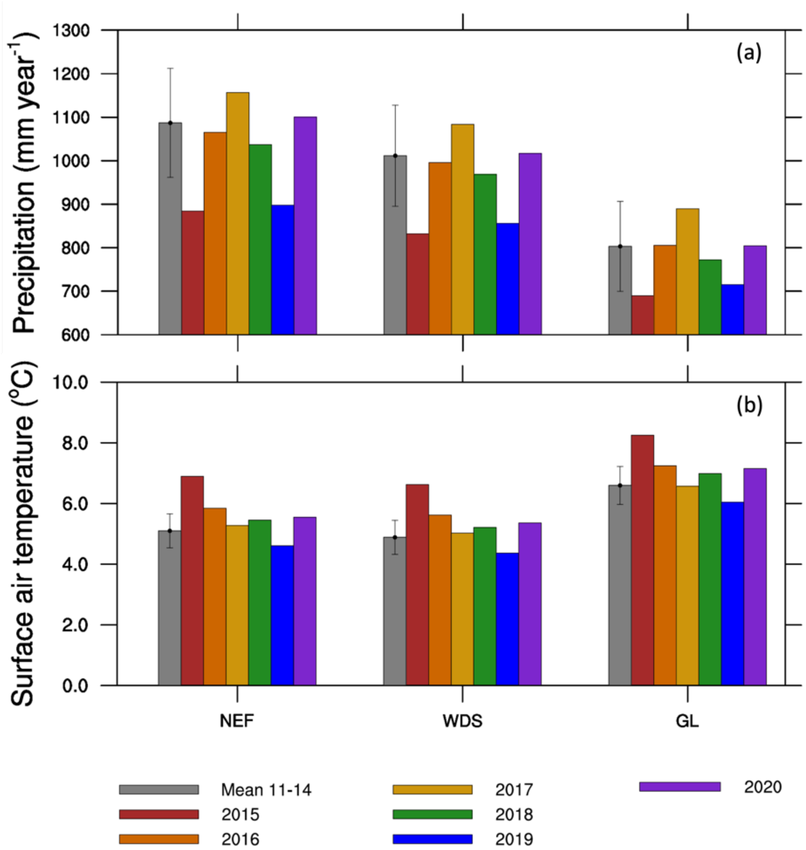

Figure 1. Mean annual (a) precipitation and (b) surface air temperature within the burned sites of the three different vegetation types. NEF: needleleaf evergreen forests, WDS: woodland savannas, and GL: grasslands. The gray bars represent the pre-fire mean values from 2011 to 2014.

3.2 LAI, GPP, and ET 2011–2020

Wildfires reduced LAI, GPP, and ET below the pre-fire mean in all VTs at the highest burn severity (herein S; S>3; Figure 2; we present results for S below 3 in Figure S6 and Table S1). The 2011–2014 growing season mean LAI values were 1.87 ± 0.10, 1.47 ± 0.04, and 1.16 ± 0.03 m^2 m^{-2} over NEF, WDS, and GL, respectively. The growing season LAI had an increasing trend from 2016 to 2020 in all the VTs, with 2020 values of 1.18, 1.04, and 0.88 m^2 m^{-2} for NEF, WDS, and

GL, respectively (Figure 2a). GPP and ET patterns were similar to those of LAI, with the highest values during 2011–2014 and the lowest values in 2016. GPP and ET in 2020 was not back up to the mean 2011–2014 values (Figures 2b and 2c). Similar but less dramatic declines in LAI, GPP, and ET were observed in the lower burn severity classes (Table 1 and Figure S6).

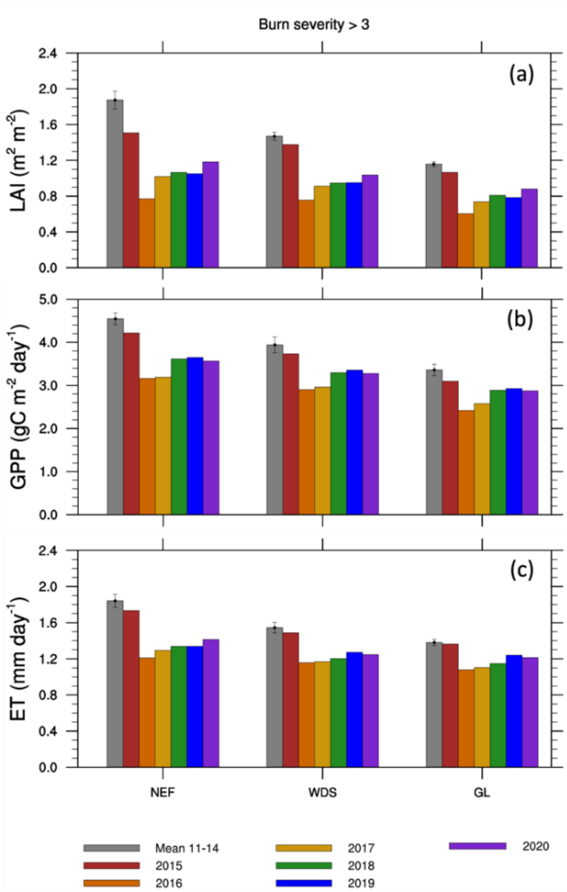

Figure 2. The growing season (a) LAI, (b) GPP, and (c) ET variation over the three vegetation types with burn severity >3 during 2011–2020. See Figure S6 for these results for fires with burn severities less than 3.

3.3 LAI, GPP, and ET resistance and resilience to wildfire

We first present wildfire resistance and resilience for each VT (using equation (1)) across the burn severity categories and present the results as a function of time further below. Resistance to wildfire declined with increasing burn severity values for LAI, GPP, and ET, and was highest for GL, intermediate for WDS, and lowest for NEF VTs, regardless of response parameter (i.e., LAI, GPP, or ET; Figures 3a, 3c, and 3e). Resilience to wildfire, calculated as the average resilience value from 2017–2020, was lower with higher burn severity for LAI, GPP, and ET (Figures 3b, 3d, and 3f). Like the patterns of resistance values, resilience was highest for GL, intermediate for WDS, and lowest for NEF. GL resilience has near 1 for all three variables in grasslands when burn severities were below 2.

Resistance and resilience calculated at the annual scale using equation (2) shows the responses of LAI, GPP, and ET relative to each other (Figure 4; S>3 shown, S values below 3 are shown in Figures S7–9). Within each VT, resistance and resilience were similar for GPP and ET, and were lower for LAI. Resistance and resilience increased for all parameters with lower burn severities (Figures S7–9), and were lowest for NEF, intermediate for WDS, and highest for GL VTs.

To examine the drivers of the interannual variation of resilience characterized by LAI, GPP, and ET, we used the random forest feature importance method to identify the contributions of precipitation, VPD, and burn severity to influencing ecosystem resilience. Burn severity was more important for NEF and WDS VTs than for GLs (Figure 5). For NEF, the importance scores of precipitation and VPD to LAI represented resilience are 0.3, while that of burn severity is 0.4 (Figure 5a). Similarly, in WDS, the importance scores of precipitation and VPD are 0.28 and 0.29, while that of burn severity is 0.43 (Figure 5b). Precipitation and VPD had relatively similar importance scores within VTs but were higher for GLs. In GL, the scores of precipitation, VPD, and burn severity to LAI represented resilience are 0.43, 0.40, and 0.16, which show the reduced importance of burn severity to GL. There are variations of important scores for GPP and ET represented resilience, and the overall conclusion of the contributions of these three metrics to the resilience values is the same between VTs. The train and test scores of different resilience values are included in Figure S10. The median R^2 scores for train and test datasets over 100 iterations ranged between 0.68–0.71 and 0.62–0.67, 0.61–0.66 and 0.54–0.61, and 0.57–0.68 and 0.57–0.64 for LAI, ET and GPP, respectively for the three VTs. As the median R^2 scores for train and test datasets are close, it suggests the model is not significantly overfitting and learning the underlying patterns in the dataset.

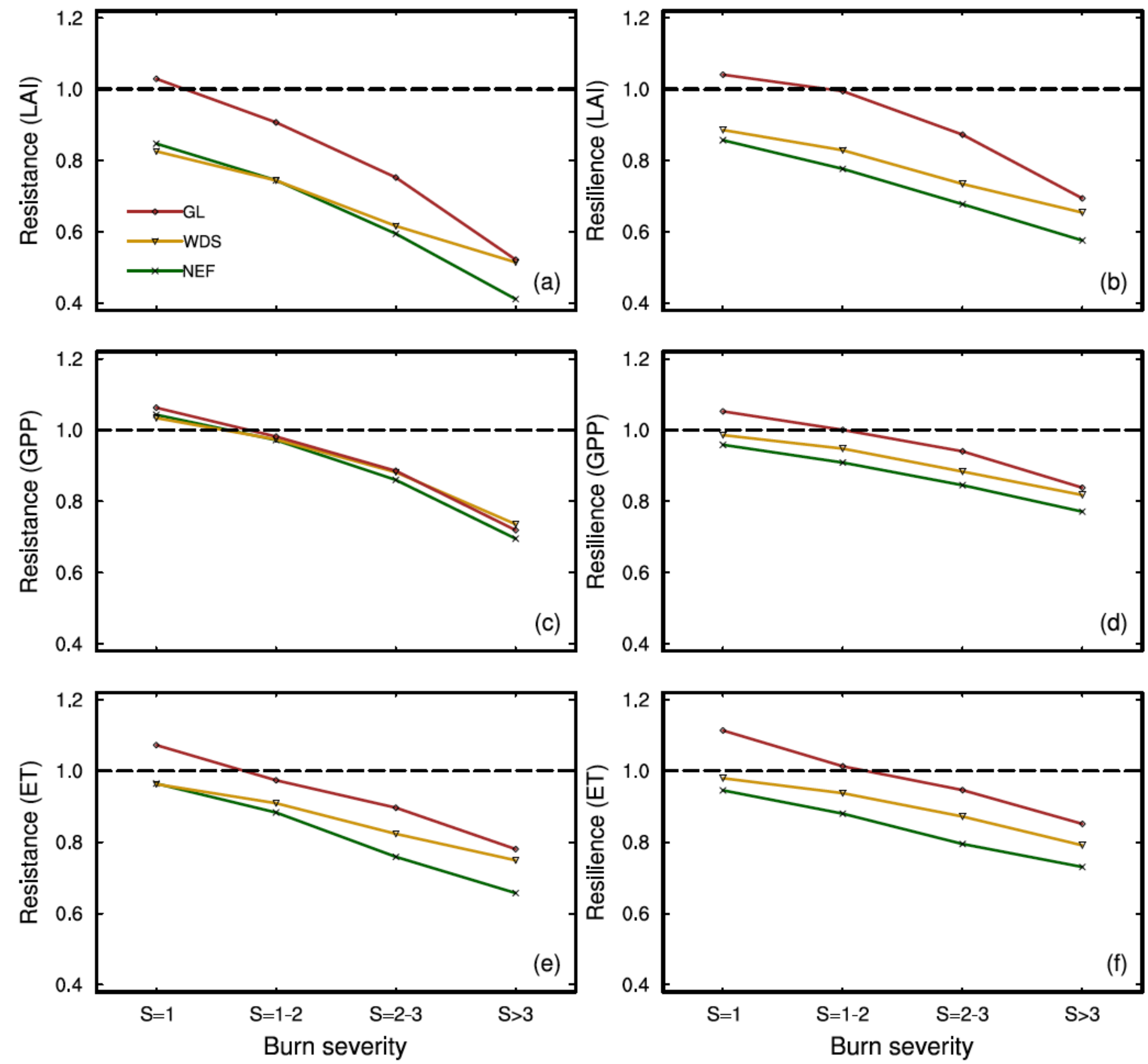

Figure 3. LAI (a) resistance and (b) resilience, GPP (c) resistance and (d) resilience, and ET (e) resistance and (f) resilience in needleleaf evergreen forests (NEF), woody savannas (WDS), and grasslands (GL) with different burn severities (Table S1). Resistance was calculated using 2016 data. The 2016 resistance are the same as those shown for S>3 in Figure (3), and are retained here to show the trends. The resilience calculation used the mean of 2017–2020.

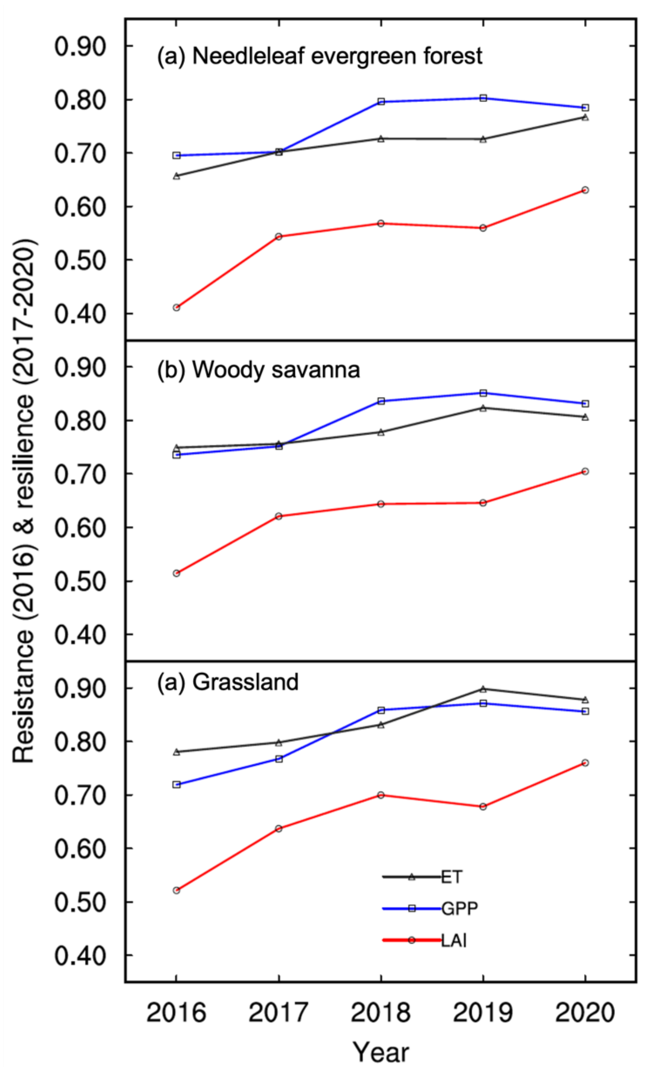

Figure 4. LAI, GPP, and ET temporal trends wildfire resistance (2016) and resilience (years 2017–2020) for (a) needleleaf evergreen forests, (b) woody savannas, and (c) grasslands with burn severity (S) larger than 3.

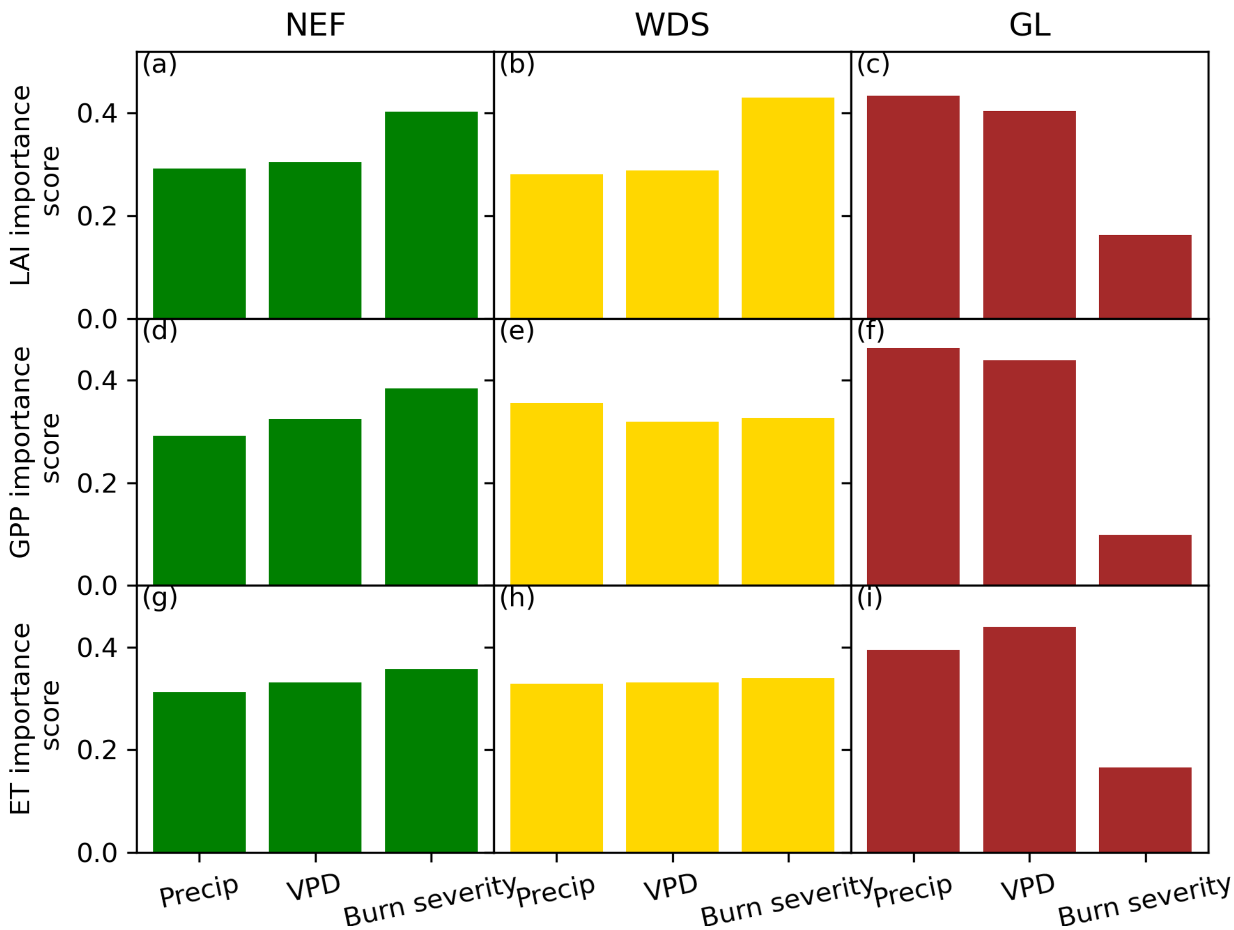

Figure 5. The feature importance of precipitation, VPD, and burn severity to resilience values in 2020 for LAI (a–c, NEF, WDS, and GL, respectively), GPP (d–f), and ET (g–i).

4. Discussion and Conclusions

This study examined the immediate impacts and subsequent recovery of vegetation to 138 wildfires with multiple burn severity levels by using remotely sensed metrics of LAI, GPP, and ET within a formal resistance and resilience framework. The random forest feature importance algorithm was used to quantify the contributions of different factors, i.e., precipitation, VPD, burn severity, to resilience. This is the first study that quantitatively assessing the post-fire resistance and resilience by simultaneously using the three MODIS products (i.e., LAI, GPP, and ET).

Overall, resistance and resilience reductions are closely related to burn severity, which matters more to the resilience of woodland VTs.

The post-fire LAI, GPP, and ET comparison between VTs shows that burn severity is a primary driver of the reductions of these three variations in all three VTs (Figures 2 and S6). This expected result occurs because the starting point of vegetation recovery one year after disturbance is set by the degree of vegetation loss. Similarly, VTs with less initial aboveground biomass and simpler ecosystem structure (i.e., GL versus NEF) recovered faster (Figures 2 and S6). This is logical because VTs with lower aboveground biomass such as grasslands are adapted to more frequent fire in part through immediate resprouting from their extensive root systems (Ratajczak et al. 2014; Isbell et al. 2015).

Resistance, or the degree of immediate impact of the wildfires, and resilience, or the degree of recovery post wildfire, were both lower as burn severity increased (Figure 3). This result quantitatively represents and findings in Figures 2 and S6, and justifies our first research hypothesis that burn severity results in lower resistance and resilience across all VTs.

Resistance and resilience were highest in GL, lowest in NEF, and intermediate in WDS (Figures 3 and 4). This result shows that the second hypothesis is valid, and supports the previous research that grasslands are better adapted to fire disturbance than other woodland types (Ratajczak et al. 2014; Isbell et al. 2015). Using equations (1) and (2), DeSoto et al. (2020) also found that gymnosperms (e.g., needleleaf forests) can have slower recovery processes than angiosperms (e.g., grasses) after drought disturbance, which can induce lower resilience values and supports our research results.

In all the resistance and resilience calculations with different MODIS products, LAI had the lowest resistance and resilience, whereas GPP and ET had similar values (Figure 4). In other words, the result justifies the recovery capacity difference between forests and grassland, and reveals that structure (i.e., LAI) has lower resistance and resilience than ecosystem fluxes (i.e., GPP and ET). These post-fire resilience features of LAI, GPP, and ET can be attributed to the evolution of different VTs to tolerate fires, where grasslands can regrow leaf area far more rapidly than forests (Ratajczak et al. 2014; Isbell et al. 2015). The results are consistent with the findings that forests tend to increase stomatal conductance and hydraulic efficiency, promoting the return of tree-scale transpiration after fires (Nolan et al. 2014). Cooper et al. (2019) also showed the enhanced transpiration rates for forests with moderate burn severity. All these findings support the relatively quicker recovery of GPP and ET, where GPP and ET respond similarly due to their tightly coupling with stomatal conductance, regulating both photosynthesis and transpiration (Knaue et al. 2020; Stoy et al. 2019). This study demonstrates that the MODIS LAI, GPP, and ET can be sufficiently used to explain resistance and resilience to wildfires in different VTs with varied burn severity at the river basin scale.

Precipitation, VPD, and burn severity had various impacts on resilience between different variables and VTs. Though the grassland showed less role of burn severity on resilience (Figure 5), the evergreen and savanna VTs showed a stronger influence of burn severity on resilience in terms of LAI. Together, these results point to higher and longer lasting impacts of wildfires on VTs with higher biomass, and precipitation, VPD, and burn severity interact in regulating ecosystem resilience. The results also show that our fourth hypothesis, expecting higher importance of precipitation and VPD to resilience in grassland than in other VTs, is testable. The post-disturbance biotic factor determined slow recovery of the forest ecosystems was also identified by Shi et al. (2017), which performed numerical simulations based on the 2005 Amazonian drought with the Community Land Model (CLM), revealing the limited influence of environmental factors to the forest recovery. The random forest feature importance study shows that hydraulics are influenced almost equally by water supply (i.e., precipitation) and demand across (i.e., VPD). Advanced studies are needed to investigate the varied impacts of precipitation and VPD on resilience in different ecosystems with various types of disturbance, which will further imply ecosystem functionality shifts due to disturbance and is beyond the scope of this study.

Overall, our research affirms the findings that obtained with plot-based measurements and shows a strong potential of using satellite observations to investigate ecosystem resistance and resilience to different types of disturbance at watershed or regional scales. It is shown by previous studies that spectral observations of forests' canopy characteristics (e.g., leaf area) tend to be biased resulting from clouds and aerosol on the measurements pathway (Asner and Alencar, 2010; Samanta et al., 2012; Xu et al., 2011). Therefore, the application of this research framework to other regions with fire disturbance, especially in the tropics with density vegetation coverages, is limited by the observational capacity of spectral-based measurements. This also implies that intensified airborne measurements and Lidar measurements can be extremely useful for enhancing the fundamental understanding of ecosystem processes after disturbances. This research paves a way for enhanced understanding of eco-hydrological processes due to various types of disturbance with satellite and airborne measurements.

With anticipated a hotter and drier fire season with extended duration in Pacific Northwest according to future climate projections (Wimberly et al. 2014), we expect that fire frequency and burn severity of wildfires will be increasing with the changing climate patterns. This study implies that with these changes, some ecosystems could have extremely low chances of a full recovery, which could induce the ecosystem degradation and carbon stock reduction. Thus, enhancing the capacity of Earth system models in reasonably predicting fires and properly characterizing the disturbance of fires is essential to the research regarding the carbon cycle, ecosystem functioning, and climate change. This research also reveals that policy makers need to develop methods, such as afforestation and sustainable agriculture, to mitigate the potential ecosystem degradation and carbon emission increase as a result of future fire disturbance.

Acknowledgements.

This research was supported by the U.S. Department of Energy (DOE), Office of Science (SC) Biological and Environmental Research (BER) program, as part of BER's Environmental System Science (ESS) program. This contribution originates from the River Corridor Scientific Focus Area (SFA) and the Interoperable Design of Extreme-scale Application Software (IDEAS)-Watershed Project at Pacific Northwest National Laboratory (PNNL). PNNL is operated for DOE by Battelle Memorial Institute under contract DE-AC05-76RL01830. This paper describes objective technical results and analysis. Any subjective views or opinions that might be expressed in the paper do not necessarily represent the views of the U.S. Department of Energy or the United States Government. This research used resources of the National Energy Research Scientific Computing Center, a DOE Office of Science User Facility supported by the Office of Science of the U.S. Department of Energy under Contract No. DE-AC02-05CH11231, using NERSC award BER-ERCAP0023098.

Conflict of Interest Statement.

All authors declare that they have no competing interests.

Data availability Statement.

The ERA5 data are at https://www.ecmwf.int/en/forecasts/dataset/ecmwf-reanalysis-v5, the MODIS products are at https://www.earthdata.nasa.gov/sensors/modis, and the MTBS data are at https://www.mtbs.gov/.

Reference.

Adams, H. D., Luce, C. H., Breshears, D. D., Allen, C. D., Weiler, M., Hale, V. C., ... & Huxman, T. E. (2012). Ecohydrological consequences of drought-and infestation-triggered tree die-off: insights and hypotheses. Ecohydrology, 5(2), 145-159.

Aires, L. M. I., Pio, C. A., & Pereira, J. S. (2008). Carbon dioxide exchange above a Mediterranean C3/C4 grassland during two climatologically contrasting years. Global Change Biology, 14(3), 539-555.

Albrich, K., Rammer, W., Turner, M. G., Ratajczak, Z., Braziunas, K. H., Hansen, W. D., & Seidl, R. (2020). Simulating forest resilience: A review. Global Ecology and Biogeography, 29(12), 2082-2096.

Asner, G. P., & Alencar, A. (2010). Drought impacts on the Amazon forest: the remote sensing perspective. New Phytologist, 187(3), 569–578.

Bart, R. R., Kennedy, M. C., Tague, C. L., & McKenzie, D. (2020). Integrating fire effects on vegetation carbon cycling within an ecohydrologic model. Ecological Modelling, 416, 108880.

Balshi, M. S., McGuire, A. D., Duffy, P., Flannigan, M., Kicklighter, D. W., & Melillo, J. (2009). Vulnerability of carbon storage in North American boreal forests to wildfires during the 21st century. Global Change Biology, 15(6), 1491-1510.

Breiman, L. (2021). Random forests. Machine Learning, 45(1), 5–32.

Cansler, C. A., & McKenzie, D. (2012). How robust are burn severity indices when applied in a new region? Evaluation of alternate field-based and remote-sensing methods. Remote Sensing, 4, 456–483.

Cooper, C. E., Aparecido, L. M., Muir, J. P., Morgan, C. L., Heilman, J. L., & Moore, G. W. (2019). Transpiration in recovering mixed loblolly pine and oak stands following wildfire in the Lost Pines region of Texas. Ecohydrology, 12(1), e2052.

DeSoto, L., Cailleret, M., Sterck, F., Jansen, S., Kramer, K., Robert, E. M. R., ... & Martínez-Vilalta, J. (2020). Low growth resilience to drought is related to future mortality risk in trees. Nat Commun, 11, 545.

Eidenshink, J., Schwind, B., Brewer, K., et al. (2007). A Project for Monitoring Trends in Burn Severity. Fire Ecology, 3, 3–21.

Falk, D. A., van Mantgem, P. J., Keeley, J. E., Gregg, R. M., Guiterman, C. H., Tepley, A. J., ... & Marshall, L. A. (2022). Mechanisms of forest resilience. Forest Ecology and Management, 512, 120129.

Friedl, M., & Sulla-Menashe, D. (2022). MODIS/Terra+ Aqua Land Cover Type Yearly L3 Global 500m SIN Grid V061. NASA EOSDIS Land Processes DAAC: Sioux Falls, SD, USA.

Jin, Y., Randerson, J. T., Goetz, S. J., Beck, P. S., Loranty, M. M., & Goulden, M. L. (2012). The influence of burn severity on postfire vegetation recovery and albedo change during early succession in North American boreal forests. Journal of Geophysical Research: Biogeosciences, 117(G1).

Jones, M. W., Smith, A., Betts, R., Canadell, J. G., Prentice, I. C., & Le Quéré, C. (2020). Climate change increases the risk of wildfires. Science Brief Review, 116, 117.

Halofsky, J. E., Peterson, D. L., & Harvey, B. J. (2020). Changing wildfire, changing forests: the effects of climate change on fire regimes and vegetation in the Pacific Northwest, USA. Fire Ecology, 16(1), 1-26.

Hersbach, H., Bell, B., Berrisford, P., Hirahara, S., Horányi, A., Muñoz-Sabater, J., ... & Thépaut, J. N. (2020). The ERA5 global reanalysis. Quarterly Journal of the Royal Meteorological Society, 146(730), 1999-2049.

Hislop, S., Jones, S., Soto-Berelov, M., Skidmore, A., Haywood, A., & Nguyen, T. H. (2019). High fire disturbance in forests leads to longer recovery, but varies by forest type. Remote Sensing in Ecology and Conservation, 5(4), 376-388.

Holling, C. S. (1973). Resilience and stability of ecological systems. Annu. Rev. Ecol. Syst., 4, 1–23.

Hu, Z., Yu, G., Fu, Y., Sun, X., Li, Y., Shi, P., ... & Zheng, Z. (2008). Effects of vegetation control on ecosystem water use efficiency within and among four grassland ecosystems in China. Global Change Biology, 14(7), 1609-1619.

Isbell, F., Craven, D., Connolly, J., Loreau, M., Schmid, B., Beierkuhnlein, C., ... & Eisenhauer, N. (2015). Biodiversity increases the resistance of ecosystem productivity to climate extremes. Nature, 526(7574), 574-577.

Knauer, J., Zaehle, S., De Kauwe, M. G., Haverd, V., Reichstein, M., & Sun, Y. (2020). Mesophyll conductance in land surface models: effects on photosynthesis and transpiration. The Plant Journal, 101(4), 858-873.

Li, F., Peng, Y., Zhang, D., Yang, G., Fang, K., Wang, G., et al. (2019). Leaf area rather than photosynthetic rate determines the response of ecosystem productivity to experimental warming in an alpine steppe. Journal of Geophysical Research: Biogeosciences, 124(7), 2277-2287.

Li, Y., Shi, H., Zhou, L., Eamus, D., Huete, A., Li, L., et al. (2018). Disentangling climate and LAI effects on seasonal variability in water use efficiency across terrestrial ecosystems in China. Journal of Geophysical Research: Biogeosciences, 123(8), 2429-2443.

McDowell, N. G., Anderson-Teixeira, K., Biederman, J. A., Breshears, D. D., Fang, Y., Fernandez-de-Una, L., et al. (2023). Ecohydrological decoupling under changing disturbances and climate. One Earth, 6(3), 251-266.

Mills, D., Jones, R., Carney, K., St. Juliana, A., Ready, R., Crimmins, A., et al. (2015). Quantifying and monetizing potential climate change policy impacts on terrestrial ecosystem carbon storage and wildfires in the United States. Climatic Change, 131, 163-178.

Myneni, R. B., et al. (2002). Global products of vegetation leaf area and fraction absorbed PAR from year one of MODIS data. Remote Sensing of Environment, 83(1–2), 214-231.

Nolan, R. H., Mitchell, P. J., Bradstock, R. A., & Lane, P. N. (2014). Structural adjustments in resprouting trees drive differences in post-fire transpiration. Tree Physiology, 34(2), 123-136.

Pechony, O., & Shindell, D. T. (2010). Driving forces of global wildfires over the past millennium and the forthcoming century. Proceedings of the National Academy of Sciences of the United States of America, 107, 19167–19170.

Picotte, J. J., Bhattarai, K., Howard, D., Lecker, J., Epting, J., Quayle, B., et al. (2020). Changes to the Monitoring Trends in Burn Severity program mapping production procedures and data products. Fire Ecology, 16, 1-12.

Poulos, H. M., Barton, A. M., Koch, G. W., Kolb, T. E., & Thode, A. E. (2021). Wildfire severity and vegetation recovery drive post-fire evapotranspiration in a southwestern pine-oak forest, Arizona, USA. Remote Sensing in Ecology and Conservation, 7(4), 579-591.

Proença, V., Pereira, H. M., & Vicente, L. (2010). Resistance to wildfire and early regeneration in natural broadleaved forest and pine plantation. Acta Oecologica, 36(6), 626-633.

Rammer, W., Braziunas, K. H., Hansen, W. D., Ratajczak, Z., Westerling, A. L., Turner, M. G., & Seidl, R. (2021). Widespread regeneration failure in forests of Greater Yellowstone under scenarios of future climate and fire. Global Change Biology, 27(18), 4339-4351.

Raymond, C. L., & McKenzie, D. (2012). Carbon dynamics of forests in Washington, USA: 21st century projections based on climate-driven changes in fire regimes. Ecological Applications, 22(5), 1589-1611.

Ratajczak, Z., Nippert, J. B., Briggs, J. M., & Blair, J. M. (2014). Fire dynamics distinguish grasslands, shrublands and woodlands as alternative attractors in the Central Great Plains of North America. Journal of Ecology, 1374-1385.

Rodman, K. C., Veblen, T. T., Andrus, R. A., Enright, N. J., Fontaine, J. B., Gonzalez, A. D., et al. (2021). A trait-based approach to assessing resistance and resilience to wildfire in two iconic North American conifers. Journal of Ecology, 109(1), 313-326.

Running, S. W., Nemani, R. R., Heinsch, F. A., Zhao, M., Reeves, M., & Hashimoto, H. (2004). A continuous satellite-derived measure of global terrestrial primary productivity: Future science and applications. Bioscience, 56, 547–560.

Samanta, A., Knyazikhin, Y., Xu, L., Dickinson, R. E., Fu, R., Costa, M. H., et al. (2012). Seasonal changes in leaf area of Amazon forests from leaf flushing and abscission. Journal of Geophysical Research: Biogeosciences, 117(G1).

Schoennagel, T., Balch, J. K., Brenkert-Smith, H., Dennison, P. E., Harvey, B. J., Krawchuk, M. A., et al. (2017). Adapt to more wildfire in western North American forests as climate changes. Proceedings of the National Academy of Sciences, 114(18), 4582-4590.

Seidl, R., & Turner, M. G. (2022). Post-disturbance reorganization of forest ecosystems in a changing world. Proceedings of the National Academy of Sciences, 119(28), e2202190119.

Seidl, R., Schelhaas, M. J., Rammer, W., & Verkerk, P. J. (2014). Increasing forest disturbances in Europe and their impact on carbon storage. Nature Climate Change, 4(9), 806-810.

Shi, M., Liu, J., Zhao, M., Yu, Y., & Saatchi, S. (2017). Mechanistic processes controlling persistent changes of forest canopy structure after 2005 Amazon drought. Journal of Geophysical Research: Biogeosciences, 122(12), 3378-3390.

Shi, M., Parazoo, N. C., Jeong, S. J., Birch, L., Lawrence, P., Euskirchen, E. S., & Miller, C. E. (2020). Exposure to cold temperature affects the spring phenology of Alaskan deciduous vegetation types. Environmental Research Letters, 15(2), 025006.

Stoy, P. C., El-Madany, T. S., Fisher, J. B., Gentine, P., Gerken, T., Good, S. P., et al. (2019). Reviews and syntheses: Turning the challenges of partitioning ecosystem evaporation and transpiration into opportunities. Biogeosciences, 16(19), 3747-3775.

Sulla-Menashe, D., & Friedl, M. A. (2018). User guide to collection 6 MODIS land cover (MCD12Q1 and MCD12C1) product. USGS: Reston, VA, USA, 1, 18.

Sun, Q., Meyer, W. S., Koerber, G. R., & Marschner, P. (2020). Rapid recovery of net ecosystem production in a semi-arid woodland after a wildfire. Agricultural and Forest Meteorology, 291, 108099.

Westerling, A. L. (2016). Increasing western US forest wildfire activity: sensitivity to changes in the timing of spring. Philosophical Transactions of the Royal Society B: Biological Sciences, 371(1696), 20150178.

Williams, A. P., Abatzoglou, J. T., Gershunov, A., Guzman-Morales, J., Bishop, D. A., Balch, J. K., & Lettenmaier, D. P. (2019). Observed impacts of anthropogenic climate change on wildfire in California. Earth's Future, 7(8), 892-910.

Wimberly, M. C., & Liu, Z. (2014). Interactions of climate, fire, and management in future forests of the Pacific Northwest. Forest Ecology and Management, 327, 270-279.

Xu, L., Samanta, A., Costa, M. H., Ganguly, S., Nemani, R. R., & Myneni, R. B. (2011). Widespread decline in greenness of Amazonian vegetation due to the 2010 drought. Geophysical Research Letters, 38(7).

Zheng, T., Martínez-Vilalta, J., García-Valdés, R., Gazol, A., Camarero, J. J., & Mencuccini, M. (2021). Disentangling biology from mathematical necessity in twentieth-century gymnosperm resilience trends. Nature Ecology & Evolution, 5(6), 733-735.